Physicochemical characterization of soiling from photovoltaic facilities in arid locations in the Atacama Desert

Pablo Ferrada[1], Douglas Olivares[1], Valeria del Campo[2], Aitor Marzo[1], Francisco Araya[1], Enrique Cabrera[3], Jaime Llanos[4], Jonathan Correa-Puerta[2], Carlos Portillo[5], Domingo Román Silva[6], Mauricio Trigo-Gonzalez[1], Joaquín Alonso-Montesinos[7,8], Gabriel López[9], Jesús Polo[10], Francisco Javier Batlles[7,8], Edward Fuentealba[1]

[1]Centro de Desarrollo Energético Antofagasta, Universidad de Antofagasta, Angamos 601, Antofagasta, Chile
[2]Departmento de Física, Universidad Técnica Federico Santa María, España 1680, Valparaíso, Chile
[3]International Solar Energy Research Center, Rudolf-Diesel Str. 15, D-78467 Konstanz, Germany
[4]Departmento de Química, Universidad Católica del Norte, Angamos #0610, Antofagasta, Chile
[5]Departamento de Ingeniería Eléctrica, Universidad de Antofagasta, Angamos 601, Antofagasta, Chile
[6]Departamento de Química, Universidad de Antofagasta, Angamos 601, Antofagasta, Chile
[7]Departmento de Química y Física, Universidad de Almería, Spain
[8]CIESOL, Joint Centre of the University of Almeria CIEMAT, 04120, Almería, Spain
[9]Departmento de Ingeniería Eléctrica y Térmica, Universidad de Huelva, Huelva, Spain
[10]Photovoltaic Solar Energy Unity (Renewable Energy Division-CIEMAT), 28040 Madrid, Spain

Tel: + 56-55-2513530, email: pablo.ferrada@uantof.cl

Abstract

Soiling is an issue that impacts the performance of photovoltaic (PV) technologies as it attenuates the amount of solar resource reaching the solar cells. The chemical composition of the soil is essential to define cleaning strategies of photovoltaic companies. This paper reports the characterization of the chemical and physical properties of the soiling deposited on photovoltaic modules located in the Atacama Desert. The particle size, shape and chemical composition of dust were studied at 4 different locations (denoted as L1 to L4) with samples taken from the ground and the module surface. It was found that, most deposited material exhibits a diameter between 1 µm and 60 µm. The determination of the particle shape factor shows that smaller particles tend to have a circular appearance, while larger particles exhibit a prismatic form. These small particles show a shape factor close to 1 and occur at the 4 locations with the greatest frequency, 40-70%. The mineral species in both the deposited and ground dust, which were identified by means of X-ray diffraction, were albite, anorthite, calcite, cristobalite, gypsum, halite, quartz, muscovite and orthoclase. The compounds occurring with the highest frequency in both the module and ground dust at all locations were quartz and anorthite. Differences between the locations were found. Calcite was found only at L3. Gypsum was not detected at L1 and L3 but was present in L2 and L4. Similarly, cristobalite was found only at L1 and L3, halite was found at L2 and L3, and muscovite was found at L1 and L2.

Keywords: soiling, particle size distribution, SEM/EDX, XRD, flat collectors

1 Introduction

With a cloudiness index of less than 3% in noncoastal areas and low atmospheric aerosol and ozone content, the Atacama Desert is one of the places with the highest levels of radiation on the planet, reaching values over 8 kWh/m^2 per day in some regions in northern Chile (Escobar et al., 2014; Larraín and Escobar, 2012; Rondanelli et al., 2015). These properties constitute ideal conditions for the proliferation of solar projects (Marzo et al., 2018). According to the New Energy Finance Climascope prepared by Bloomberg New Energy Finance and the International Development Bank, Chile had reached first place for renewable energy investments in Latin America and the Caribbean (Bloomberg New Energy Finance, 2016). These facts resulted in record investment of 3.2 billion

dollars. Along with this emerging development and high growth, there are new challenges and problems strictly linked to the geographical conditions of the region. Among these issues its extreme aridity, high salinity, low rainfall, the influence of the Pacific Ocean, the impact of industrial mining activities.

One of the main concerns for photovoltaic (PV) modules, especially in a desert environment, is soiling. The affects the optimal operation of a PV system (Mehmood et al., 2017). Soiling can be defined as layers of dust or dirt that accumulate on the surface of PV modules, resulting in power generation losses.

When studying losses in PV production, it is important to consider optimal locations for determining the best emplacement for PV plants (Marzo et al., 2017). Researchers have studied these processes for several decades (Sarver et al., 2013), and recently, exhaustive reviews have been written about soiling mechanisms (Figgis et al., 2017), as well as the effects of dirt accumulation on the output power of PV modules (Costa et al., 2018). In addition, soiling affects other solar energy technologies, including solar thermal power and concentrated solar power (CSP) (Sayyah et al., 2013) (Bouaddi et al., 2017). Both PV modules and solar thermal flat collectors use solar glass as the front surface. Consequently, soiling characterization is relevant for both cases (Said, 1990).

The dust deposited on PV modules is harmful in most places around the world, especially in arid areas (Qasem et al., 2014). Accumulated dust on PV modules creates a layer on the optical surface. This layer causes optical losses, reducing the number of photons that reach the solar cells, and leading to the consequential diminution of their performance. The optical losses are due to the absorbance, reflectance and dispersion of the incident light because of the presence of dust (Sayyah et al., 2014). Arid areas with windy and dusty environments may intensify soiling. Studies (Sarver et al., 2013) have shown that for arid regions, a shorter time can lead to the same performance reduction generated after months in regions with more temperate and tropical climates. In semiarid and arid desert regions, rainfall is scarce so there is no natural cleaning of the modules. Further, in some cases, humidity reinforces the adhesion and cementation of dust on PV surfaces (Ilse et al., 2016). In deserts near the ocean such as the Atacama Desert, a dense fog often appears in the morning. This fog reduces the direct component of solar radiation (Sayyah et al., 2014) and supports adhesion based on the hygroscopic property of dust to attract humidity (Bateman et al., 2014)(Figgis et al., 2016). Soiling effects on the energy yield in the Atacama Desert were recently reported (Cordero et al., 2018). The measurements carried out for one year revealed peak energy losses of 39% in the northern coastal part of the desert; while, at relatively high-altitude sites and in the southern part of the desert losses were 3% or less.

To evaluate the impact of soiling, the performance ratio PR, which is the ratio of the actual and theoretically possible energy outputs, can be used as metric of the quality of a PV plant independent of location. This evaluation showed significantly decreased values in the Atacama Desert. Researchers (Araya et al., 2016) have evaluated the PR for different locations in the desert, including coastal locations, an industrial site and the Andean plateau. They found that over a 12-months period, the PR degradation was slightly higher for multicrystalline silicon (mc-Si, 47%) compared to cadmium telluride, CdTe, thin film modules (46%) at the coastal zone. Another comparison by same authors revealed that an amorphous/microcrystalline silicon (a-Si/μc-Si) thin films (51%) led to the largest decrease in PR, followed by mc-Si (39%), and the smallest decrease in PR occurred in monocrystalline silicon (mono Si) modules (36%), which were also at the coastal zone of the desert. Conversely, the same calculation for modules installed at an industrial location in an inner region of the desert resulted in PRs of 53% for CdTe, 49% for mc-Si and 47% for mc-Si with 1-axis tracking. The rate by which the PR degraded

over time depended on technology, installation, temperature and location. Figure 1 depicts the PR degradation for one of the selected locations of this work (Location L2, as an example, according to the map in Fig. 2).

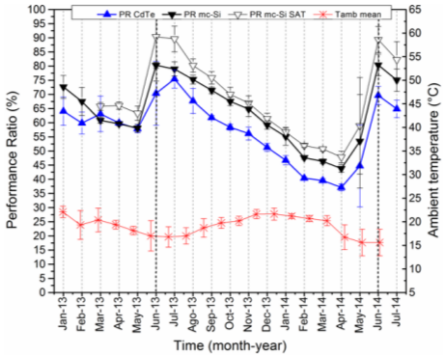

Fig. 1. Performance ratio and mean ambient temperature as function of time. The technologies are installed at L2 and consist of CdTe at fixed angle (5.6 kWp), mc-Si at a fixed angle (5.52 kWp) and mc-Si with 1-axis tracking (5.52 kWp).

The effects of soiling on the spectral transmittance for different PV technologies have been studied (Qasem et al., 2014). It was found that the transmittance variation of samples installed at 30º showed a nonuniformity of 4.4% compared to 0.2% at 90º. The transmittance decreased for wavelengths below 570 nm where large band gap technologies (thin films) were more affected. In terms of photo-generated current density (J_{ph}), the worst case was amorphous silicon (a-Si) with a 33% decrease, whereas crystalline silicon (c-Si) exhibited a 28.6% reduction in J_{ph} when dust surface density was 4.25 mg/cm^2. The work of (Said and Walwil, 2014) showed a 20% reduction in the glass transmittance when the dust density was 5 g/m^2 (0.5 mg/cm^2), which was obtained after 45 days with PV modules tilted at 26º from the latitude of Dhahran.

The degree by which dust particles hinder the optimal performance of PV modules can depend on their physical and chemical properties, such as the chemical composition, size, shape (Pulipaka and Kumar, 2018)(Johnson et al., 1971)(Nelson et al., 2011) and distribution over the glass surface (K. K. Ilse et al., 2018)(Ostuka et al., 1988). Using resuspension theory based on the adhesion force, hydrodynamic force and torque for rolling detachment, researchers (Jiang et al., 2018) have studied the impact of the wind speed and the resuspension of soiling having particle sizes in the range of 0.1 to 100 µm on the flat surface of a PV module. The resuspension of particles exhibiting a diameter from 0.1 to 100 µm was enable for a shear velocity and wind velocity of 0.23 to 58 m/s and 0.8 to 2220 m/s, respectively. The authors in (Pulipaka et al., 2016) used the particle size distribution to model the PV soiling losses based on regression analysis and neuronal networks. Particles with sizes of 75 µm or less had the greatestt impact on the power output at irradiance levels in the range of 300 to 500 W/m^2, whereas the 150 µm particles had the greatest impact on the power output at irradiances between 1000 and 1200 W/m^2.

The authors in (Xingcai and Kun, 2018) developed a model based on fundamental physics concepts, namely, the Lambert-Beer law, to predict the effects of particle size distributions on the transmittance of the PV glass. They concluded that it is necessary to take the material nature, concentration and particle size distribution into account to achieve a correct forecasting of the dusty glass transmittance of PV modules. Depending on the diameter (d) of dust particles, wavelength (λ) and refractive index (n), it is possible to define a criterion for determining which scattering mechanism describes light-matter interactions. In a review by (Ghazi et al., 2014), three cases are recognized: (i) For

$\pi d/\lambda < 0.6/n$ holds, scattering is governed by Reyleigh's theory. (ii) For $\pi d/\lambda > 0.6$, reflection applies. (iii) For $0.6/n < \pi d/\lambda < 0.6$, scattering is given by Mie's theory.

Regarding soil types, researchers (John et al., 2016) collected dust from six locations and deposited the dust artificially in the laboratory. One of their experiments consisted of measuring losses with the dust types, where each has an equal density of 1.8 g/cm^2 on several PV technologies. In all cases, the largest losses were measured in the 300-600 nm spectral range for various soil types. Therefore, this is the spectral range where the highest peak in the incident solar spectrum of AM 1.5 G is found, and this research shows that the dust type exhibiting the highest spectral sensitivity in this wavelength range leads to the highest soiling loss.

As expected, the transmittance and PV performance have been modeled while considering dust properties. However, these investigations mainly correlate the transmittance and PV performance with the particles size, and the other physical and chemical properties are neglected.

This work focuses on the physical and chemical characterization of the soiling dust particles from 4 locations within the Atacama Desert. These locations represent different environmental conditions, such as coastal desert, desert and an industrial-mining desert area. Additionally, the dust obtained from the PV modules is compared to the ground dust at the different locations. Characterization of the dust particles is mainly performed with optical microscopy and X-ray diffraction, since it is mainly focused on the size, shape and mineral composition. Scanning electron microscopy (SEM) and energy dispersive spectroscopy (EDX) measurements of the ground and module dust at each location are also reported in this study. This characterization can be used to perform subsequent studies on the optical and electrical losses in laminated solar cells under simulated indoor conditions (as shown by (Burton and King, 2014)) and/or PV devices exposed outdoors.

2 Materials and methods

2.1 Locations and installations

The soiling study was carried out at four locations in the Atacama Desert, and samples were enumerated from north to south, L1 to L4, as shown in Fig. 2. A description of each location is seen in Table 1, giving information about the geographic locations. Climates in the Atacama Desert are classified as hyper arid, arid, semi-arid and sub humid zones (Hartley et al., 2005). According to this classification, the large PV plant (L1), the industrial location L2, and the Solar Platform of the Atacama Desert or PSDA (L4) are located in the arid zone at the central depression, whereas Antofagasta (L3) is located in the hyper arid zone at the coastal zone. Characterization of the soiling, such as the particle size, morphology, and the chemical composition of the soil, was performed for the dust samples collected at L1-L4 from the module surface and from the ground (see Table 1 for details on the installations from where the samples were taken).

The dust present on the module surface was collected by using a hard filament brush with the ability to drag deposited dust. All material was taken from the top to the bottom of the module surface. After that, the particles were stored in plastic bags and brought to the laboratory. The dust from the ground at locations L1-L4 was collected by using a plastic spoon and stored in plastic bags. Samples were sonicated in an ultrasonic cleaner for approximately 40 min and quartered.

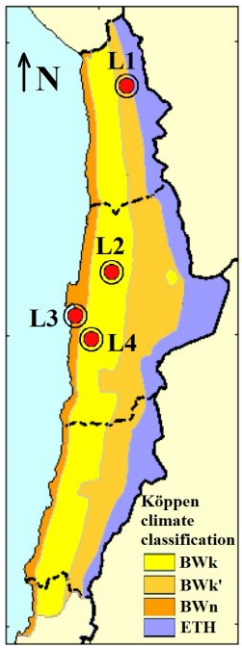

Fig. 2. Map of northern Chile. The total length of the country is approximately 4300 km. The rectangle depicts a portion of the Atacama Desert and the geographical distribution of the studied locations: a large PV plant (L1), an industrial location (L2), Antofagasta (L3) and the Solar Platform of Atacama Desert or PSDA (L4). The legend uses the Köppen climate classification (Kottek et al., 2006).

Table I: Characteristics of location L1-L4. At L1 there is a 2 MW mc-Si PV plant with 1-axis tracking. At L2 there are 3 PV plants, namely, a 5.6 kW CdTe module at a fixed angle, a 5.52 mc-Si module at a fixed angle and a 5.52 mc-Si module with 1-axis tracking. At L3 there are 3 plants consisting of 3.36 kW a-Si/µc-Si, 3.33 mc-Si and 3.33 monocrystalline Si. At L4 there are c-Si technologies adding up to approximately 20 kW.

	Name	Latitude	Longitude	Altitude (m)	Climate
L1	Large PV plant	18.45°S	69.88°W	1660	BWk'
L2	Industrial location	23.43°S	69.50°W	1600	BWk
L3	Antofagasta city	23.70°S	70.42W	50	BWn
L4	PSDA	24.09°S	69.93°W	1000	BWk

2.2 Measurement tools and equipment

2.2.1 Optical microscopy

For the size analysis and its examination of the relationship with the particle morphology, we used an optical microscope (Leica DM IRB). This microscope gives a digital image with the size bar already included. Images were taken with a 20x magnification and analyzed with ImageJ software. We analyzed more than 200 particles of dust from the ground and module of each location. From the image analysis with the software we obtained the following characteristics: the area (A), perimeter (P), circularity (C_0) and aspect ratio (C_t). The particle aspect ratio, C_t, is related to its area and to its longest projection (L), where L is the parameter we use as the definition of particle size, and, which is obtained through the following equation:

$$L = \sqrt{\frac{4AC_t}{\pi}} \qquad \text{Eq. (1)}$$

2.2.2 Scanning electron microscopy

To analyze the morphology of the smallest particles and determine the elemental composition of the dust samples, scanning electron microscopy (SEM) and energy dispersive X-ray spectrometry (EDX) microanalysis was performed with a Jeol JSM-6360 LV SEM, which was equipped with an energy dispersive spectrometer (Oxford Inca C200). Using EDX, we analyzed more than 200 particles from the soil of each location. To calculate the relative amount of each element at each location, measurements were averaged.

2.2.3 Rotary micro riffler

To obtain a representative sample from each bag, the dust was processed with a rotary micro riffler from Quantachrome. The spinning riffler device uses mechanical (vibrational) energy to provide a constant flow of material from its holder. The steady flow passes through a divider head that rotates at a constant speed, minimizing segregation. The amplitude of the vibratory motion and the velocity of the circular motion can be controlled separately. The latter allows different powders having varying flow characteristics to be subdivided. After this process, each sample can be analyzed separately or recombined to yield a representative sample.

2.2.4 X-ray diffraction

Powder X-ray diffraction (PXRD) was used to characterize dust collected from the module surface and the ground at the PV installation site. Data were collected with a Bruker AXS D8 Advance Diffractometer in the 2θ range from 10º to 60º, with CuKα radiation (λ=0.15045 pm) at 40 kV and 30 mA. Measurements were carried out at room temperature. The qualitative analysis was performed by using the Powder Diffraction File, PDF-4, Database (Kabekkodu et al., 2002).

3. Physics of soiling

3.1 Particle size and morphology

Dust samples were collected from the ground and module surface at each location for optical microscopy, SEM and EDX analysis. Optical microscopy was used to analyze the particle size and shape. Figure 3 shows the particle size distribution for the locations.

At L1 (location furthest north), the particle size is between 1 and 130 μm; however, 98% of all particles are smaller than 50 μm, and therefore, this analysis focuses on that size. Particles smaller than 10 μm are most commonly found in the ground samples and not on the module as expected. This result seems to imply the preferential deposition of particles with sizes between 10 and 30 μm on the module surface. At L2 (the industrial zone), a similar behavior is observed; 75% of the ground particles are between 1 and 10 μm, but only 56% of module particles are in this range. A noticeable preferential deposition of large particles is observed with a larger amount of the module particles having sizes between 10 and 50 μm.

At L3 (the coast), 93% of the particles are smaller than 50 μm, 5% are between 50 and 100 μm, and the rest are larger particles reaching sizes of 200 μm. Therefore, the analysis focuses on particles smaller than 50 μm, since the number of larger particles is almost equivalent (1%) for all ranges between 50 and 100 μm. The size distributions of the dust from L3 differs from that from L1 and L2. In this case, there is a preferential deposition of particles with sizes between 1 and 10 μm on the module surface (62%). A similar behavior is observed for L4; dust particles smaller than 10 μm account for 76% at the

module surface, while 60% of the ground dust is in this size range. This outcome could imply that a different deposition mechanism occurs at L1 and L2 compared to L3 and L4. To further understand this phenomenon, the particle morphology of the dust collected at these locations is analyzed.

To quantify the particle morphology, the shape factor (A_{shape}) is calculated. This parameter is defined as the inverse of the particle circularity and associated with the complexity of the particle. The shape factor is calculated with Eq. 2, where P and A are the perimeter and area of the particle, respectively. Both parameters are obtained by image analysis performed with ImageJ software. A shape factor of unity corresponds to a perfect circle.

$$A_{shape} = \frac{P^2}{4\pi A} \tag{2}$$

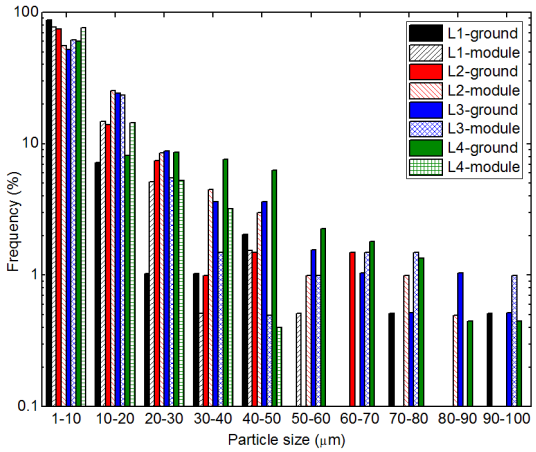

Fig. 3. Particle size distribution histogram of the ground and module dust.

The average shape factor is between 1.2 and 1.5 for all locations, which is in good agreement with reports of samples of similar sizes from other locations (Reid, 2003)(Yilbas et al., 2015). Figure 4a shows the A_{shape} histogram of the dust at all locations, and Fig. 4b depicts the relationship between the shape factor and particle size). In Fig. 5, the SEM microphotographs of particles are shown.

At L1, more than 30% of the dust particles (32% of ground samples and 36% of module samples) are perfect circles (A_{shape}=1), and most of the particles are almost circular, i.e., their shape factor is between 0.9 and 1.1. The ground and module dust show almost the same number of particles with A_{shape} smaller than 1.2, adding up to 70% of all particles. A large number of circular particles on the module surface (a higher proportion compared to the ground) could explain the large proportion of particles larger than 10 μm found on the module. It seems that, in this case, particle deposition is driven by the particle shape, more than size. This preferential deposition of circular particles agrees with previous work, showing that the noncircular particle shape slows deposition (Figgis et al., 2017).

At L2, the number of circular particles (A_{shape}=1) is almost the same for the ground and module dust. The ground dust at L2 shows a larger number of particles with a shape factor between 0.9 and 1.1 compared to the module dust from the same location (55% and 46%, respectively). In this case (at L2), small particles from the ground and module (below 10 μm) exhibit a similar relationship between the shape factor and particle size. Therefore, there are more particles in the ground dust than the module dust with an A_{shape} value near 1, which agrees with our finding that a large number of ground particles had sizes smaller than 10 μm. The module dust at L2 has more particles with a shape factor larger than 1.2

compared to the ground dust. At the same time, there are more particles between 10 and 50 μm due to the close relationship between the particle size and shape, as observed in Fig. 4b. Therefore, the greater deposition of noncircular particles at L2 is consistent with a preferential deposition of particles larger than 10 μm. However, this behavior is not expected and, in this case, implies the presence of particles having larger shape factors. L2 is an industrial site, so some of the deposited dust may have come from this source, rather than from the ground dust near the modules.

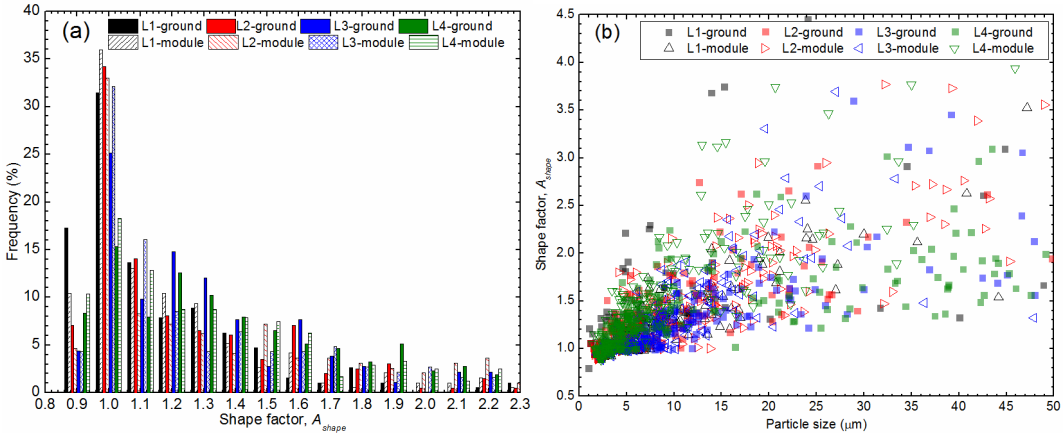

Fig. 4a. Particles shape factor distribution histogram of the ground (full columns) and module (shaded columns) dust from all locations. Fig. 4b: Shape factor as a function of particles size for the ground (full markers) and module (empty markers) dust from the locations.

At L3, circular particles account for 25% and 32% of the ground and module dust, respectively. This difference increases when considering particles with A_{shape} between 0.9 and 1.1, which accounts for 39% and 52% of the ground and module dust, respectively. Dust from L3 shows a slow change in the shape factor as a function of size, so the preferential deposition of small particles (less than 10 μm) implies the presence of an even larger number of almost circular particles in the module dust.

L4 has the lowest number of circular particles (15% and 18% of the ground and module dust, respectively) and a larger shape distribution than that of the other study locations. In this case, there are more module particles with a shape factor between 0.9 and 1.1 than there are ground particles in this range; particles with a shape factor between 0.9 and 1.1 account for 42% and 32% of the module and ground dust, respectively. This important difference is also observed in the number of particles smaller than 20 μm. Particles smaller than 10 μm were expected to deposit preferentially, yet this expectation was not conclusively shown in this case; therefore, as shown at L1, the dust deposition is driven by the particle shape more than by the size. For further analysis of the small particles found at each location, we performed scanning electron microscopy (Fig. 5). The dust shape is heterogeneous at all locations, and the lack in uniformity is seen in the module dust. In all cases, the main observed geometry is prismatic; however, L1, L2 and L4 also have layered particles. The number of layered particles is higher in the module dust than in the ground dust for these three locations, showing the preferential deposition of these type of particles with this geometry. In location L3 the existence of particles with needle-like rod shape can be observed.

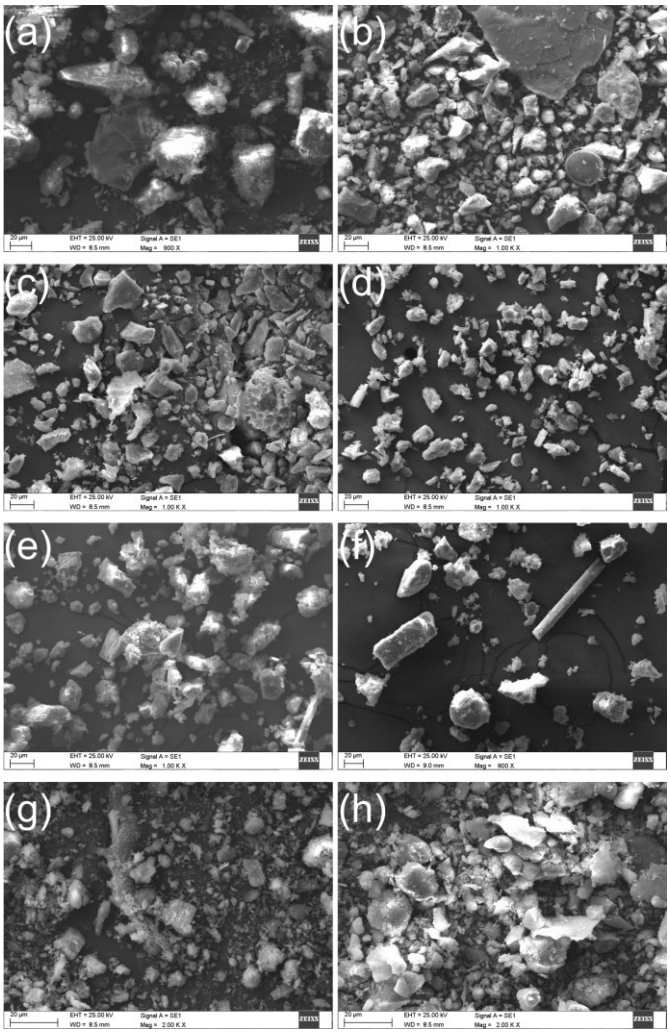

Fig. 5. Scanning electron microscope images of the dust particles collected from the ground (a, c, e, and g) and module (b, d, f, h) at locations L1 (a and b), L2 (c and d), L3 (e and f) and L4 (g and h).

3.2 Chemical composition

3.2.1 Elemental identification

To study the elemental composition of the soil from the different locations, we performed energy dispersive X-ray spectroscopy on the ground dust. The results shown in Fig. 6 correspond to the elemental analysis of the soils collected from L1, L2, L3 and L4. The species found in large quantities (more than 1% in almost all cases) represent the composition of samples collected from the Earth's crust containing O^{-2}, Si^{+4}, Al^{+3}, Fe^{+3}, Fe^{+2}, Ca^{+2}, Mg^{+2}, Na^{+} and K^{+} ions, making up 98.5% of the soil (Mile and Mitkova, 2012). In addition, Cl^{-} was found.

One of the characteristics of the soil in the Atacama Desert is the salinity, which occurs due to the presence of sulfates, chlorides, and oxides (Ewing et al., 2006). According to Ewing et al 2006, most of the hyper arid soil has accumulated atmospheric salts including, sulfates and chlorides. The compounds within the mineral species can be in the form of precipitated crystals or found between the interstitial spaces a trace level, as was the case of the copper found at L3.

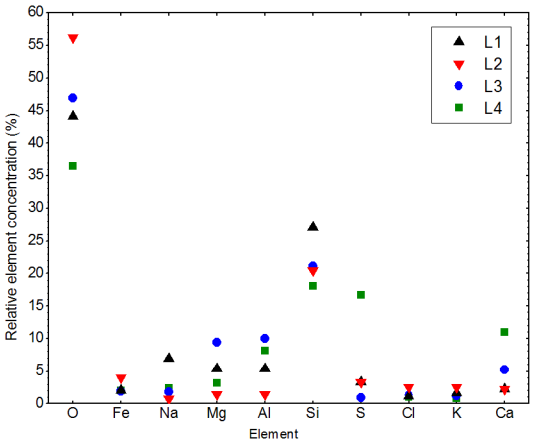

Fig. 6. Elemental analysis of samples from the ground of L1 (black triangles), L2 (red inverted triangles), L3 (blue circles) and L4 (green squares).

As expected, the main element, besides oxygen, is silicon for all the locations. In addition to Si, the samples collected at L4 have a significant amount of S (17%) and Ca (12%) compared to the other locations. The largest quantity of Na (7%) is observed in the samples collected from L1 and the largest amounts of Mg (10%) are detected in the samples collected from L3. The other elements are found in similar concentrations at all locations. Since the locations considered for this study are separated by more than 100 km, the chemical composition of the soils associated with each site was expected to be different. Therefore, physical characteristics such as the color and texture, and chemical properties, such as the salinity, conductivity and pH, may also be important.

3.2.2 Mineral identification

Several types of minerals are present in the dust samples collected at L1-L4. The types of materials, found at each location, are rock remnants already consolidated after years of geological processes that have generated minerals and soils with different properties. Therefore, it is important to determine the crystalline species present in each sample.

The mineral compositions of the ground and module dust collected from L1-L4 were determined via PXRD. The samples were found to contain following minerals: (a) albite ($NaAlSi_3O_8$), (b) anorthite ($CaAl_2Si_2O_8$), (c) calcite ($CaCO_3$), (d) cristobalite (SiO_2), (e) gypsum ($CaSO4{\cdot}2H_2O$), (f) halite (NaCl), (g) quartz (SiO_2), (h) muscovite $KAl_2(AlSi_3O_{10})(OH)_2$ and (i) orthoclase ($KAlSi_3O_8$). The letters (a) to (i) are used in the diffractograms in Fig. 7, which shows the mineral species found at all the locations.

According to the XRD analysis and the study locations, different minerals are found in the Atacama Desert. This is in good agreement with the authors of (Marquet et al., 1998), who report on a number of ecosystems in the Atacama Desert, which are influenced by the coast, arid regions and the Andean Plateau. These regions have different geological characteristics that determine soil properties such as the color and salinity. Nevertheless, the major compounds are observed at all the locations. These minerals are albite, anorthite, quartz and orthoclase. Regarding the differences between the locations, Calcite stands out, as it was present only at L3 (Figures 5g and 5m). Calcium was present as anorthite in all locations (including L3), and gypsum was present in L2 and L3. Cristobalite was found at L1 and L3 but not at L2 and L4. Halite was detected only at L2 and L3; since Na and Cl were detected at all locations, it is probable that the amount of NaCl at L1 and L4 is too low. Finally, muscovite was also detected at two locations, L1 and L2. Potassium found at L3 and L4 is present as orthoclase, also found at L1 and L2.

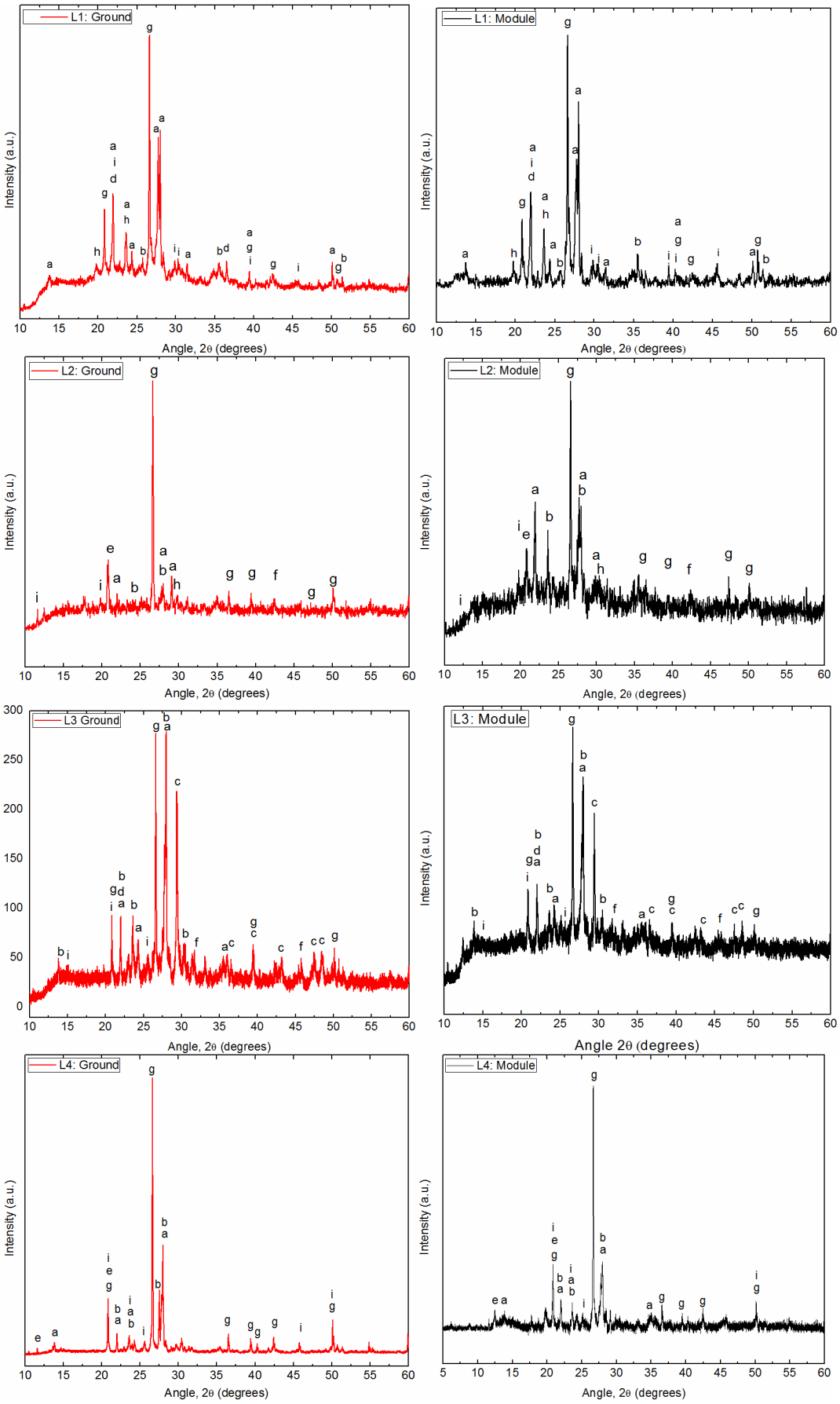

Fig. 7. X-ray diffraction for samples collected at L1-L4 from the ground (red) and from the module surface (black).

The samples collected from the ground and module surface were also compared for each location. In our case, no significant differences were found between the composition of samples from the module surface and the ground (Fig. 7). This result suggests that the depositing dust corresponds to material coming from the location. Regarding L1, the main differences between the ground and module dust was the presence of albite and muscovite, which were both found in a larger amount in the ground at L1. At L2, anorthite produce a large peak at 23.6 degrees in the diffractogram for the ground dust, while the same is almost negligible in the module dust. Calcite, only present at L3, also shows differences between the ground and module; it is a major component of the module dust. Contrary to L2, at L4, a larger amount of anorthite is presence in module dust than in the ground dust. Table II gives an overview of the major species.

Table II: Summary of the species detected by PXRD for the dust samples collected at locations L1 to L4 from the module surface (M) and ground (G).

Mineral	L1-M	L1-G	L2-M	L2-G	L3-M	L3-G	L4-M	L4-G
Albite	✓	✓	✓	✓	✓	✓	✓	✓
Anorthite	✓	✓	✓	✓	✓	✓	✓	✓
Calcite					✓	✓		
Cristobalite	✓	✓			✓	✓		
Gypsum			✓	✓			✓	✓
Halite			✓	✓	✓	✓		
Quartz	✓	✓	✓	✓	✓	✓	✓	✓
Muscovite	✓	✓	✓	✓				
Orthoclase	✓	✓	✓	✓	✓	✓	✓	✓

4. Discussion

We could establish that most of the deposited particles were in the range of 1-10 µm for all the locations and decreased in number for larger sizes up to 90-100 µm. Less than 1% of particles were larger than 100 µm. For a given particle size range, most particles can be either in the ground or on the module surface, depending on the location. This suggests the preferential deposition of particles for a given size range. However, generalization is impossible since it depends on the location. The shape factor for small particles (<10 µm) was 1.1 at all locations and varies between 1.8 and 2.3 for large particles (>10 µm). For a given particle size, the presence of more particles in the ground or on module surface also depends on the location. The results show that the smaller the particle, the more circular the shape.

An investigation performed in Qatar found a shape factor near 1 for small particles and 3.5 for large particles (Aïssa et al., 2016). Other authors measured a mean value of 3 for samples collected from the Sahara Desert. In the range where most of the area and volume exist, A_{shape} was 1.4. The shape factor can be analyzed for specific properties such as the density and chemical composition. For instance, the authors in (Reid, 2003) report on earlier studies, which demonstrated A_{shape} values of 1.12, 1.27 and 1.32 for chained spheres, 1.36-1.82 for quartz, 2.04 for talc and 1.57 for sand-like species. Similarly, particles exhibiting a particular shape are rich in certain elements. Researchers showed that quadrangular particles initially deformed from a cubic shape were rich in sodium and chlorine, whereas aggregated particles were rich in calcium and oxygen (Dulieu et al., 2013). In the case of particles having flake-like shapes, the particles were composed of calcium and silicon (Yilbas et al., 2015).

In the search of major compounds, the same minerals were present in the ground and on the module surface. However, there were difference between the locations. Each

location can have differences in the particle size distribution and shape factor for particles collected from the ground and module. Regarding composition, the locations revealed differences in the major compounds present. Conversely, the major compounds detected in the particles collected from the ground and module surface correspond to each other.

Soiling particles interact differently depending on the solubility of the mineral supporting an interaction with water droplets. A recent work (K. Ilse et al., 2018) compared the dust surface coverage and transmittance of soiled glass in indoor and outdoor conditions. The indoor test was carried out by using a soiling chamber, whereas the outdoor experiment consisted of studying 4 glass types having different coatings during 5 months at the PSDA location (L4). The authors found that the soling layer is formed or "caked" by the accumulation and compaction of minerals (with particle sizes larger than 4 μm) during dew cycles, in which water-soluble salts support dust particle adhesion to the module surface (K. K. Ilse et al., 2018). A higher adhesion force of the dust particles to the PV glass was measured for material concentrations that chemically bind the particle to the surface under the influence of water and possibly ultraviolet light (Kazmerski et al., 2016). Using microtribometer, the force needed to remove dry mud from a glass surface was 5 times higher than from a polycarbonate substrate (Mehmood et al., 2017). The cause was attributed to the high cohesive forces that result from the dried mud solution at the interface between the mud and glass. These authors pointed out that the dust particles consisted of a nonuniform distribution of Na, K, Mg, Ca, O_2 and Fe (our analysis, shown in Fig. 6, depicts the same elements).

Information regarding the particle size, shape and composition can be useful to determine how to clean glass surfaces, since the adhesion forces are dependent on these characteristics (Figgis et al., 2018). Accordingly, the main factors affecting the dust deposition are: the particle size, shape, composition (including the hygroscopic properties), relative humidity, surface-dew point and surface wettability.

There are several reviews outlining the effects of soiling on the optical and electrical performance of PV modules, including mitigation strategies (Costa et al., 2018; Figgis et al., 2018; Sarver et al., 2013). Partially shaded module surfaces present another key issue regarding the operation of PV modules. Soiling or dust particle accumulation can lead to this condition. Under soft shading conditions produced by soiling, the output current will be decreased, while the output voltage does not vary much. Conversely, in hard shading conditions, when the dust layer becomes thick and dense, the PV module performance is dependent on whether some solar cells are shaded or all of them are shaded (Maghami et al., 2016). Maghami et al showed the effect of partial shading on the current-voltage (IV) characteristics of PV modules. The impact of soiling on the performance ratio was depicted by Fig. 1, in the introduction section. For the site corresponding to L2, see Fig. 2 in the materials and methods section. We performed IV measurements for two different conditions of the PV installations at L2 (see Fig. 2): clean and dirty conditions (where the dirty condition corresponds to 10 months of dust accumulation). The results are shown in Table III. A similar methodology was applied in (Ye et al., 2014).

The values shown in Table III indicate that the current was the most affected by the dust since it was reduced, by at least, 40% (both the short circuit and MPP current). Conversely, the voltage (open circuit and MPP voltage) and the fill factor only decreased by, at most, 5%. As a result, the output power decreased by up to 45%, which was mostly due to the changes in the generated current.

Table III: Percentage degradation of the electrical parameters due to 10 months of dust accumulation. The installed capacities were 5.52 kWp for CdTe and 5.52 kWp for the mc-Si plants.

	CdTe, β=25º	mc-Si, β=25º	mc-Si with tracking
$(I_{sc.c}-I_{sc.d})/I_{sc.c}$	43.8	40.1	39.6
$(I_{mpp.c}-I_{mpp.d})/I_{mpp.c}$	44.1	43.6	44.0
$(V_{oc.c}-V_{oc.d})/V_{oc.c}$	3.1	3.3	4.8
$(V_{mpp.c}-V_{mpp.d})/V_{mpp.c}$	1.1	-0.9	0.3
$(FF_c-FF_d)/FF_c$	-2.9	1.4	2.7
$(P_{out,c}-P_{out,d})/P_c$	44.7	43.1	44.2

The selection of locations covers an important portion of the Atacama Desert, which exhibits BWn and BWk climates, according to the Köppen classification. The results presented in this study provided insights on the role of the particle size, shape and composition. Nevertheless, the results are limited and cannot be applied to the whole Atacama Desert due to its large size and mineral richness. In future work, it will be necessary to carry out new sampling, including more sites to be representative of the entire region in terms of the soil types. This can be achieved if the goal is to determine the origin of the dust deposited on the modules. In addition, more samples per location from both the ground and module surface would allow for performing chemical quantification via powder XRD and the TOPAS (Total Pattern Analysis Solution) approach (Rajiv et al., 2010).

5. Conclusion

This work provided fundamental information about the physical and chemical properties of the soil particles deposited on the surface of PV modules and those collected from the ground in the Atacama Desert. The selected locations for the study represent different types of climates within the territory (L1-L4). For all locations, the particles described as perfect circles, were present in the largest amounts; however, the morphology distribution varies from site to site and between the ground and module. At L1, the particle deposition is mainly driven by shape rather than size; while at L3 there is a preferential deposition of particles smaller than 10 μm. At L2 some of the module particles may come from nearby industry, since they are larger and more amorphous than expected. However, this assumption could not be corroborated by X ray diffraction analysis. L4 has the smallest number of circular particles in the ground and module dust. Therefore, it is not possible to standardize a homogeneous size for the whole Atacama Desert. The mineral composition analyzed for the samples from the ground and module surface is similar for each location, showing no significant qualitative distinctions. There are differences mainly in the size and shape, which is probably due to weather conditions; however, further quantitative studies have to be performed r to compare other physical and chemical properties of the dust. From a global perspective, the comparison of size, morphology and mineral composition of the dust from each of the four locations suggests that each site exhibits different characteristics.

Acknowledgment

The authors acknowledge MINEDUC-UA project codes ANT 1755, CONICYT/ FONDAP/ 15110019 "Solar Energy Research Center" SERC-Chile, the Chilean Economic Development Agency (CORFO) with contract No 17PTECES-75830 under the framework of the project “AtaMoS TeC” and the Unidad de Equipamiento Científico “MAINI” of the Universidad Católica del Norte for the support in the preparation of

samples, analysis and generation of data through the XRD team, and FIC-Regional Project EQU-25 Conicyt 2009-2010. In addition, we acknowledge at international level the Federal Ministry of Education and Research (BMBF, Germany) for their "Solar Collaboration between Chile and Deutschland (Solar Child)" project No 01DN14005, as well as the Spanish Ministry of the Economy, Industry and Competitiveness "PVcastsoil" project Nº ENE2017-83790-C3-1-2-3-R in collaboration with the European Regional Development Fund.

References

Aïssa, B., Isaifan, R.J., Madhavan, V.E., Abdallah, A.A., 2016. Structural and physical properties of the dust particles in Qatar and their influence on the PV panel performance. Sci. Rep. 6, 1–12. https://doi.org/10.1038/srep31467

Araya, F., Ferrada, P., Rabanal-Arabach, J., Marzo, A., Fuentealba, E., 2016. Performance Analysis of Photovoltaics Systems Installed at Different Sites in the Atacama Desert, in: 32nd European Photovoltaic Solar Energy Conference and Exhibition. WIP, pp. 1635–1640. https://doi.org/10.4229/EUPVSEC20162016-5CO.14.6

Bateman, A.P., Belassein, H., Martin, S.T., 2014. Impactor apparatus for the study of particle rebound: Relative humidity and capillary forces. Aerosol Sci. Technol. 48, 42–52. https://doi.org/10.1080/02786826.2013.853866

Bloomberg New Energy Finance, 2016. The Clean Energy Country Competitiveness Index. Clim. 2016 91.

Bouaddi, S., Ihlal, A., Fernández-García, A., 2017. Comparative analysis of soiling of CSP mirror materials in arid zones. Renew. Energy 101, 437–449. https://doi.org/10.1016/j.renene.2016.08.067

Burton, P.D., King, B.H., 2014. Spectral sensitivity of simulated photovoltaic module soiling for a variety of synthesized soil types. IEEE J. Photovoltaics 4, 890–898. https://doi.org/10.1109/JPHOTOV.2014.2301895

Cordero, R.R., Damiani, A., Laroze, D., MacDonell, S., Jorquera, J., Sepúlveda, E., Feron, S., Llanillo, P., Labbe, F., Carrasco, J., Ferrer, J., Torres, G., 2018. Effects of soiling on photovoltaic (PV) modules in the Atacama Desert. Sci. Rep. 8, 13943. https://doi.org/10.1038/s41598-018-32291-8

Costa, S.C.S., Diniz, A.S.A.C., Kazmerski, L.L., 2018. Solar energy dust and soiling R&D progress: Literature review update for 2016. Renew. Sustain. Energy Rev. 82, 2504–2536. https://doi.org/10.1016/j.rser.2017.09.015

Dulieu, F., Congiu, E., Noble, J., Baouche, S., Chaabouni, H., Moudens, A., Minissale, M., Cazaux, S., 2013. How micron-sized dust particles determine the chemistry of our Universe. Sci. Rep. 3. https://doi.org/10.1038/srep01338

Escobar, R.A., Cortés, C., Pino, A., Pereira, E.B., Martins, F.R., Cardemil, J.M., 2014. Solar energy resource assessment in Chile: Satellite estimation and ground station measurements. Renew. Energy 71, 324–332. https://doi.org/10.1016/J.RENENE.2014.05.013

Ewing, S.A., Sutter, B., Owen, J., Nishiizumi, K., Sharp, W., Cliff, S.S., Perry, K., Dietrich, W., McKay, C.P., Amundson, R., 2006. A threshold in soil formation at Earth's arid-hyperarid transition. Geochim. Cosmochim. Acta 70, 5293–5322. https://doi.org/10.1016/j.gca.2006.08.020

Figgis, B., Ennaoui, A., Ahzi, S., Rémond, Y., 2017. Review of PV soiling particle mechanics in desert environments. Renew. Sustain. Energy Rev. 76, 872–881. https://doi.org/10.1016/j.rser.2017.03.100

Figgis, B., Ennaoui, A., Guo, B., Javed, W., Chen, E., 2016. Outdoor soiling microscope for measuring particle deposition and resuspension. Sol. Energy 137, 158–164. https://doi.org/10.1016/j.solener.2016.08.015

Figgis, B., Nouviaire, A., Wubulikasimu, Y., Javed, W., Guo, B., Ait-Mokhtar, A., Belarbi, R., Ahzi, S., Rémond, Y., Ennaoui, A., 2018. Investigation of factors affecting condensation on soiled PV modules. Sol. Energy 159, 488–500. https://doi.org/10.1016/j.solener.2017.10.089

Ghazi, S., Sayigh, A., Ip, K., 2014. Dust effect on flat surfaces - A review paper. Renew. Sustain. Energy Rev. 33, 742–751. https://doi.org/10.1016/j.rser.2014.02.016

Hartley, A.J., Chong, G., Houston, J., Mather, A.E., 2005. 150 million years of climatic stability: evidence from the Atacama Desert, northern Chile. J. Geol. Soc. London. 162, 421–424. https://doi.org/10.1144/0016-764904-071

Ilse, K., Khan, M.Z., Naumann, V., Hagendorf, C., 2018. LABORATORY SOILING TESTING FOR EVALUATION OF ANTI-SOILING COATING PERFORMANCE 1–23.

Ilse, K., Werner, M., Naumann, V., Figgis, B.W., Hagendorf, C., Bagdahn, J., 2016. Microstructural analysis of the cementation process during soiling on glass surfaces in arid and semi-arid climates.

598 Phys. Status Solidi - Rapid Res. Lett. 10, 525–529. https://doi.org/10.1002/pssr.201600152
599 Ilse, K.K., Rabanal, J., Schönleber, L., Khan, M.Z., Naumann, V., Hagendorf, C., Bagdahn, J., 2018.
600 Comparing indoor and outdoor soiling experiments for different glass coatings and microstructural
601 analysis of particle caking processes. IEEE J. Photovoltaics 8, 203–209.
602 https://doi.org/10.1109/JPHOTOV.2017.2775439
603 Jiang, Y., Lu, L., Ferro, A.R., Ahmadi, G., 2018. Analyzing wind cleaning process on the accumulated
604 dust on solar photovoltaic (PV) modules on flat surfaces. Sol. Energy 159, 1031–1036.
605 https://doi.org/10.1016/j.solener.2017.08.083
606 John, J.J., Warade, S., Tamizhmani, G., Kottantharayil, A., 2016. Study of soiling loss on photovoltaic
607 modules with artificially deposited dust of different gravimetric densities and compositions
608 collected from different locations in India. IEEE J. Photovoltaics 6, 236–243.
609 https://doi.org/10.1109/JPHOTOV.2015.2495208
610 Johnson, K.L., Kendall, K., Roberts, A.D., 1971. Surface Energy and the Contact of Elastic Solids. Proc.
611 R. Soc. A Math. Phys. Eng. Sci. 324, 301–313. https://doi.org/10.1098/rspa.1971.0141
612 Kabekkodu, S.N., Faber, J., Fawcett, T., IUCr, 2002. New Powder Diffraction File (PDF-4) in relational
613 database format: advantages and data-mining capabilities. Acta Crystallogr. Sect. B Struct. Sci. 58,
614 333–337. https://doi.org/10.1107/S0108768102002458
615 Kazmerski, L.L., Diniz, A.S.A.C., Maia, C.B., Viana, M.M., Costa, S.C., Brito, P.P., Campos, C.D.,
616 Neto, L.V.M., de Morais Hanriot, S., de Oliveira Cruz, L.R., 2016. Fundamental Studies of
617 Adhesion of Dust to PV Module Surfaces: Chemical and Physical Relationships at the Microscale.
618 IEEE J. Photovoltaics 6, 719–729. https://doi.org/10.1109/JPHOTOV.2016.2528409
619 Kottek, M., Grieser, J., Beck, C., Rudolf, B., Rubel, F., 2006. World map of the Köppen-Geiger climate
620 classification updated. Meteorol. Zeitschrift 15, 259–263. https://doi.org/10.1127/0941-
621 2948/2006/0130
622 Larraín, T., Escobar, R., 2012. Net energy analysis for concentrated solar power plants in northern Chile.
623 Renew. Energy 41, 123–133. https://doi.org/10.1016/J.RENENE.2011.10.015
624 Maghami, M.R., Hizam, H., Gomes, C., Radzi, M.A., Rezadad, M.I., Hajighorbani, S., 2016. Power loss
625 due to soiling on solar panel: A review. Renew. Sustain. Energy Rev. 59, 1307–1316.
626 https://doi.org/10.1016/j.rser.2016.01.044
627 Marquet, P.A., Bozinovic, F., Bradshaw, G.A., Cornelius, C., Gonzalez, H., Gutierrez, J.R., Hajek, E.R.,
628 Lagos, J.A., Lopez-Cortes, F., Nunez, L., Rosello, E.F., Santoro, C., Samaniego, H., Standen, V.G.,
629 Torres-Mura, J.C., Jaksic, F.M., 1998. The Atacama desert ecosystems and adjacent Andean area in
630 northern Chile. Rev. Chil. Hist. Nat. 71 593-617. 593–617.
631 Marzo, A., Ferrada, P., Beiza, F., Besson, P., Alonso-Montesinos, J., Ballestrín, J., Román, R., Portillo,
632 C., Escobar, R., Fuentealba, E., 2018. Standard or local solar spectrum? Implications for solar
633 technologies studies in the Atacama desert. Renew. Energy 127.
634 https://doi.org/10.1016/j.renene.2018.05.039
635 Marzo, A., Trigo, M., Alonso-Montesinos, J., Martínez-Durbán, M., López, G., Ferrada, P., Fuentealba,
636 E., Cortés, M., Batlles, F.J., 2017. Daily global solar radiation estimation in desert areas using daily
637 extreme temperatures and extraterrestrial radiation. Renew. Energy 113.
638 https://doi.org/10.1016/j.renene.2017.01.061
639 Mehmood, U., Al-Sulaiman, F.A., Yilbas, B.S., 2017. Characterization of dust collected from PV
640 modules in the area of Dhahran, Kingdom of Saudi Arabia, and its impact on protective transparent
641 covers for photovoltaic applications. Sol. Energy 141, 203–209.
642 https://doi.org/10.1016/j.solener.2016.11.051
643 Mile, M., Mitkova, T., 2012. Soil Moisture Retention Changes in Terms of Mineralogical Composition of
644 Clays Phase. Clay Miner. Nat. – Their Charact. Modif. Appl. Many 101–118.
645 https://doi.org/http://dx.doi.org/10.5772/48098
646 Nelson, A., Keene, S., Diaz, J.M., Susca, E., Nazarian, D., Gonzales, E., Kennedy, C.E., 2011.
647 Understanding soil adhesion in Concentrating Solar Power plants: a novel analysis of soil
648 characteristics. SolarPaces Conf.
649 Ostuka, A., Iida, K., Danjo, K., Sunada, H., 1988. NII-Electronic Library Service. Chem. Pharm. Bull. 36,
650 741–749. https://doi.org/10.1248/cpb.37.3229
651 Pulipaka, S., Kumar, R., 2018. Analysis of soil distortion factor for photovoltaic modules using particle
652 size composition. Sol. Energy 161, 90–99. https://doi.org/10.1016/j.solener.2017.11.041
653 Pulipaka, S., Mani, F., Kumar, R., 2016. Modeling of soiled PV module with neural networks and
654 regression using particle size composition. Sol. Energy 123, 116–126.
655 https://doi.org/10.1016/j.solener.2015.11.012
656 Qasem, H., Betts, T.R., Muellejans, H., AlBusairi, H., Gottschalg, R., 2014. Dust-induced shading on
657 photovoltaic modules. Prog. Photovolt Res. Appl. 22, 218–226.

https://doi.org/https://doi.org/10.1002/pip
Rajiv, P., Dinnebier, R.E., Jansen, M., 2010. “Powder 3D Parametric”- A program for Automated Sequential and Parametric Rietveld Refinement Using Topas. Mater. Sci. Forum 651, 97–104. https://doi.org/10.4028/www.scientific.net/MSF.651.97
Reid, J.S., 2003. Comparison of size and morphological measurements of coarse mode dust particles from Africa. J. Geophys. Res. 108, 8593. https://doi.org/10.1029/2002JD002485
Rondanelli, R., Molina, A., Falvey, M., 2015. The Atacama surface solar maximum. Bull. Am. Meteorol. Soc. 96, 405–418. https://doi.org/10.1175/BAMS-D-13-00175.1
Said, S.A.M., 1990. Effects of dust accumulation on performances of thermal and photovoltaic flat-plate collectors. Appl. Energy 37, 73–84. https://doi.org/10.1016/0306-2619(90)90019-A
Said, S.A.M., Walwil, H.M., 2014. Fundamental studies on dust fouling effects on PV module performance. Sol. Energy 107, 328–337. https://doi.org/10.1016/j.solener.2014.05.048
Sarver, T., Al-Qaraghuli, A., Kazmerski, L.L., 2013. A comprehensive review of the impact of dust on the use of solar energy: History, investigations, results, literature, and mitigation approaches. Renew. Sustain. Energy Rev. 22, 698–733. https://doi.org/10.1016/j.rser.2012.12.065
Sayyah, A., Horenstein, M.N., Mazumder, M.K., 2014. Energy yield loss caused by dust deposition on photovoltaic panels. Sol. Energy 107, 576–604. https://doi.org/10.1016/j.solener.2014.05.030
Sayyah, A., Horenstein, M.N., Mazumder, M.K., 2013. Mitigation of soiling losses in concentrating solar collectors. Conf. Rec. IEEE Photovolt. Spec. Conf. 480–485. https://doi.org/10.1109/PVSC.2013.6744194
Xingcai, L., Kun, N., 2018. Effectively predict the solar radiation transmittance of dusty photovoltaic panels through Lambert-Beer law. Renew. Energy 123, 634–638. https://doi.org/10.1016/j.renene.2018.02.046
Ye, J.Y., Reindl, T., Aberle, A.G., Walsh, T.M., 2014. Performance degradation of various PV module technologies in tropical Singapore. IEEE J. Photovoltaics 4, 1288–1294. https://doi.org/10.1109/JPHOTOV.2014.2338051
Yilbas, B.S., Ali, H., Khaled, M.M., Al-Aqeeli, N., Abu-Dheir, N., Varanasi, K.K., 2015. Influence of dust and mud on the optical, chemical, and mechanical properties of a pv protective glass. Sci. Rep. 5, 1–12. https://doi.org/10.1038/srep15833